Journal of Materials Chemistry A

ROYAL SOCIETY OF CHEMISTRY

PAPER

View Article Online
View Journal | View Issue

Check for updates

Cite this: J. Mater. Chem. A, 2024, 12, 6438

Hollow structural materials derived from a MOFs/polymer loaded CoRu alloy for significantly boosting electrochemical overall water splitting†

Yin Hu, Congcong Wang, Ying Liu, Hongyan Lin and Kai Zhang *

Received 6th November 2023
Accepted 1st February 2024

DOI: 10.1039/d3ta06794g

rsc.li/materials-a

The development of efficient and stable bifunctional electrocatalysts for overall water splitting is essential to solve the energy crisis and environmental problems. Herein, the paper reports a CoRu@N-doped carbon hollow nanostructure (CoRu@NCHNS) material by using MOFs as precursors and adding dopamine (DA) to introduce Ru and N atoms and fabricate hollow structures in one step. Thanks to the synergistic effect of the CoRu alloy, unique hollow structure and N atoms, the material achieves a current density of 10 mA cm^{-2} in the hydrogen evolution reaction (HER) and oxygen evolution reaction (OER) with very low overpotentials of 13 mV and 238 mV, respectively. In addition, an overall water splitting device was also assembled using CoRu@NCHNSs-8 h and CoRu@NCHNSs-9 h as the anode and cathode under alkaline conditions, and a current density of 10 mA cm^{-2} was obtained at a cell voltage of 1.56 V. This work explores the applications of a hollow structure loaded CoRu alloy in overall water splitting and provides a new idea for the preparation of efficient electrocatalytic overall water splitting materials.

Introduction

The rapid consumption of fossil energy will lead to a series of energy crises and environmental problems, and hydrogen energy has received a lot of attention from scientists as an efficient and clean energy source that is expected to replace traditional fossil energy sources.[1–3] Electrolysis of water, consisting of two half-reactions, the oxygen evolution reaction (OER) and hydrogen evolution reaction (HER), is considered to be one of the most promising and sustainable methods for hydrogen production.[4–7] Currently, the most efficient HER and OER electrocatalysts are Pt-based and Ir-based materials, but they are scarce and expensive, which has prompted a search for elements with similar properties to Pt but more abundant as catalysts.[8–10]

In fact, various electrocatalysts based on transition metals and their derivatives (such as metal sulfide compounds,[11,12] metal phosphides,[13–15] metal selenides,[16] metal oxides,[17] metal hydroxides,[18–20] layered double hydroxides[21,22] and so on) have been investigated as bifunctional electrocatalysts for overall water splitting, and significant progress has been made. In our previous work, CoP@NCHNCs were prepared and showed good OER and HER activities at 10 mA cm^{-2} requiring only low overpotentials of 304 mV and 93 mV. CoP@NCHNCs can be used as the anode and cathode up to 10 mA cm^{-2} at 1.62 V.[23] However, due to the complexity of the preparation process and the generation of toxic substances, further optimization is still required. D. Jason Riley and colleagues synthesized a Ni–Co@Fe–Co PBA material that exhibited significant electrocatalytic HER performance in alkaline freshwater and simulated seawater with overpotentials of 43 and 183 mV, respectively.[24] However, due to single function and poor activity, this catalyst still cannot meet the needs of practical applications. Therefore, it is still challenging to develop efficient electrocatalytic materials for overall water splitting.

Ruthenium, a platinum-based metal, has similar properties to Pt but is about 1/30 of the price. Many studies have demonstrated that Ru has excellent adsorption capacity for both OER and HER intermediates.[25,26] By the synergistic effect of transition metals and ruthenium, it is possible to achieve both a lower cost and a significant increase in catalytic activity, and is expected to be a bifunctional catalyst.[27,28] For example, Chen and colleagues have designed a cobalt single atom incorporated in a ruthenium oxide sphere material, using a Co single atom to modify the electronic structures of the surrounding Ru atoms and thereby remarkably elevate the electrocatalytic activities. The catalyst requires ultralow overpotentials, 45 mV for the HER and 200 mV for the OER, to deliver a current density of 10 mA cm^{-2}.[29]

Usually, the introduction of Ru into transition metal MOF materials was performed by ion exchange. The MOFs are immersed in a solution of Ru^{3+}, and subsequently the MOFs are etched to allow the Ru^{3+} to be exchanged with the transition metal.[30,31] For example, Qi *et al.* synthesized heterostructured

State Key Laboratory of Supramolecular Structure and Materials, College of Chemistry, Jilin University, Qianjin Street 2699, Changchun 130012, People's Republic of China. E-mail: zk@jlu.edu.cn; Fax: +86-431-85193423

† Electronic supplementary information (ESI) available. See DOI: https://doi.org/10.1039/d3ta06794g

inter-doped ruthenium–cobalt oxide [(Ru–Co)O_x] hollow nanosheet arrays by this method.[32] Electrodeposition was also an effective method to introduce Ru.[33] For example, Zhao *et al.* synthesized Ru-Pt_{rich}Co nanowires by electrodeposition.[34] In addition to this, *in situ* growth and template methods were also some common approaches.[35,36] However, these methods were either atomically underutilized or difficult to carry out. There is an urgent need to find a new and efficient method. It is well known that dopamine (DA) has a strong coordination effect on metals, and the use of dopamine to introduce Ru can greatly improve atomic utilization.[37,38] At the same time, dopamine is rich in N, and at high temperatures, it can generate pyrrole N and pyridine N to improve the electrical conductivity and modulate the electronic structure of materials.[23,39,40] Therefore, it is widely used as a ligand for electrocatalysts.

In summary, this manuscript describes the synthesis of an N-doped carbon hollow nanostructure material (CoRu@NCHNSs) based on a composite of MOFs and PDA. The material possesses a hollow structure and is loaded with the CoRu alloy. ZIF-67 provided the template and the transition metal. DA was polymerized while disassembling ZIF-67 to form a hollow structure, while introducing N atoms and utilizing strong coordination to enhance the Ru payload in one step. The hollow structure exposes more metal active sites; the introduction of N atoms improves the electrical conductivity; the introduction of small amounts of Ru induces the formation of the CoRu alloy, which greatly improves the electrocatalytic performance of the material and provides a new idea for the preparation of efficient electrocatalytic overall water splitting materials.

Experimental

It has been provided in the ESI.†

Results & discussion

Synthesis and characterization

A typical synthetic route of CoRu@NCHNSs is illustrated in Fig. 1a (for details see the ESI†). Taking CoRu@NCHNSs-9 h as an example, first, purple ZIF-67 solid powder was synthesized by leaving $Co(NO_3)_2 \cdot 6H_2O$ and 2-methylimidazole in methanol solution for 12 hours. Transmission electron microscopy (TEM) showed that ZIF-67 had a regular dodecahedral morphology with a size of 300–500 nm (Fig. 1b), which could also be seen by scanning electron microscopy (Fig. S1a†). Subsequently, ZIF-67 was dispersed in methanol, and dopamine (DA) and $RuCl_3 \cdot xH_2O$ were added and refluxed at 60 °C for 9 h to produce CoRu/PDA HNSs-9 h. The strong coordination between monomer DA and cobalt ions disassembled the structure of ZIF-67 and released alkaline 2-methylimidazole, and the alkaline conditions triggered the polymerization of DA on the surface of ZIF-67 to form a polydopamine (PDA) shell.[41,42] Moreover, Ru^{3+} was also introduced into the PDA shell due to the strong coordination between DA and Ru ions. Finally, hollow CoRu/PDA HNS materials loaded with Co and Ru ions were generated. CoRu/PDA HNSs-9 h was pyrolyzed at 750 °C under an Ar atmosphere to obtain CoRu@NCHNSs-9 h powder. The TEM image (Fig. 1c) and the breakage of the samples in the SEM image (Fig. S1b†) indicated that CoRu/PDA HNSs-9 h mostly maintained the original ZIF-67 morphology and had an obvious hollow structure. However, the surface of CoRu/PDA HNSs-9 h was rough, which was caused by the generation of small PDA particles. After pyrolysis, CoRu@NCHNSs-9 h still retained a hollow structure (Fig. 1d and S1c†), which could expose more active sites. A large number of nanoparticles was generated, which was due to the ability of the organic ligand to act as a reducing agent at high temperatures, reducing metal ions to metal monomers and nanoparticles to improve the electrical conductivity.[43–46] 0.21 and 0.23 nm lattice spacings could be observed in HR-TEM images (Fig. 1e), which was attributed to hexagonal CoRu (002) and CoRu (100) facets,[28,47–49] and indicated that MOFs and a PDA shell could act as a growth template for CoRu alloy NPs. In addition, EDS elemental mapping further confirmed the uniform distribution of Ru, Co and N atoms in the material (Fig. S2†), and illustrated the successful introduction of Ru and N.

Subsequently, a series of products at different reaction times were synthesized, CoRu@NCHNSs-7 h, CoRu@NCHNSs-8 h and CoRu@NCHNSs-10 h. It could be seen that all the CoRu/PDA HNSs were able to maintain a similar hollow structure, although the PDA shell became thicker as the reaction proceeded from 7 h to 9 h (Fig. S3a–d†). However, when the reaction proceeded to 10 h, the hollow structure was no longer independent, and the shells aggregated together. This also led to the collapse of the hollow CoRu@NCHNSs-10 h after pyrolysis (Fig. S3e and f†). As a comparison, using a similar preparation approach, Co@NCHNSs-9 h without $RuCl_3 \cdot xH_2O$ and ZnRu@NCHNSs-9 h with a similar size ZIF-8 as the template were also prepared. In short, they both had similar hollow structures (Fig. S4 and S5†).

X-ray photoelectron spectroscopy (XPS) measurements of CoRu@NCHNSs-9 h, Co@NCHNSs-9 h and ZnRu@NCHNSs-9 h were conducted to investigate the element composition and altered surface electronic structures. The XPS survey spectrum of CoRu@NCHNSs-9 h revealed the presence of Co, Ru, O, N and C elements (Fig. 2a). Similarly, the presence of C, N, O, Zn and Ru could also be observed in ZnRu@NCHNSs-9 h (Fig. S6†) and the presence of C, N, O and Co, in Co@NCHNSs-9 h (Fig. S7†). As shown in Fig. 2b, the N1s spectra of CoRu@NCHNSs-9 h had 4 characteristic peaks at 399.17 eV, 400.47 eV, 401.05 eV, and 401.74 eV, corresponding to pyridine N, pyrrole N, graphitized N and N–H bonds, respectively.[28,30,49] The interaction of Co and Ru was investigated by comparing the high-resolution XPS spectra of CoRu@NCHNSs-9 h, ZnRu@NCHNSs-9 h and Co@NCHNSs-9 h. First, the Co $2p_{3/2}$ characteristic peaks in the high-resolution Co 2p XPS spectrum of CoRu@NCHNSs-9 h were at 779.16 eV and 780.70 eV, which were attributed to Co^0 and Co^{2+} species (Fig. 2b),[49–51] respectively. It was shifted to a higher binding energy than the Co^{2+} peak (780.39 eV) in Co@NCHNSs-9 h (Fig. S8b†), which was mainly due to the electron transfer from Co to Ru in the CoRu alloy. And the high-resolution XPS spectrum of Ru 3p in CoRu@NCHNSs-9 h showed that Ru$3p_{3/2}$ shifted toward a lower

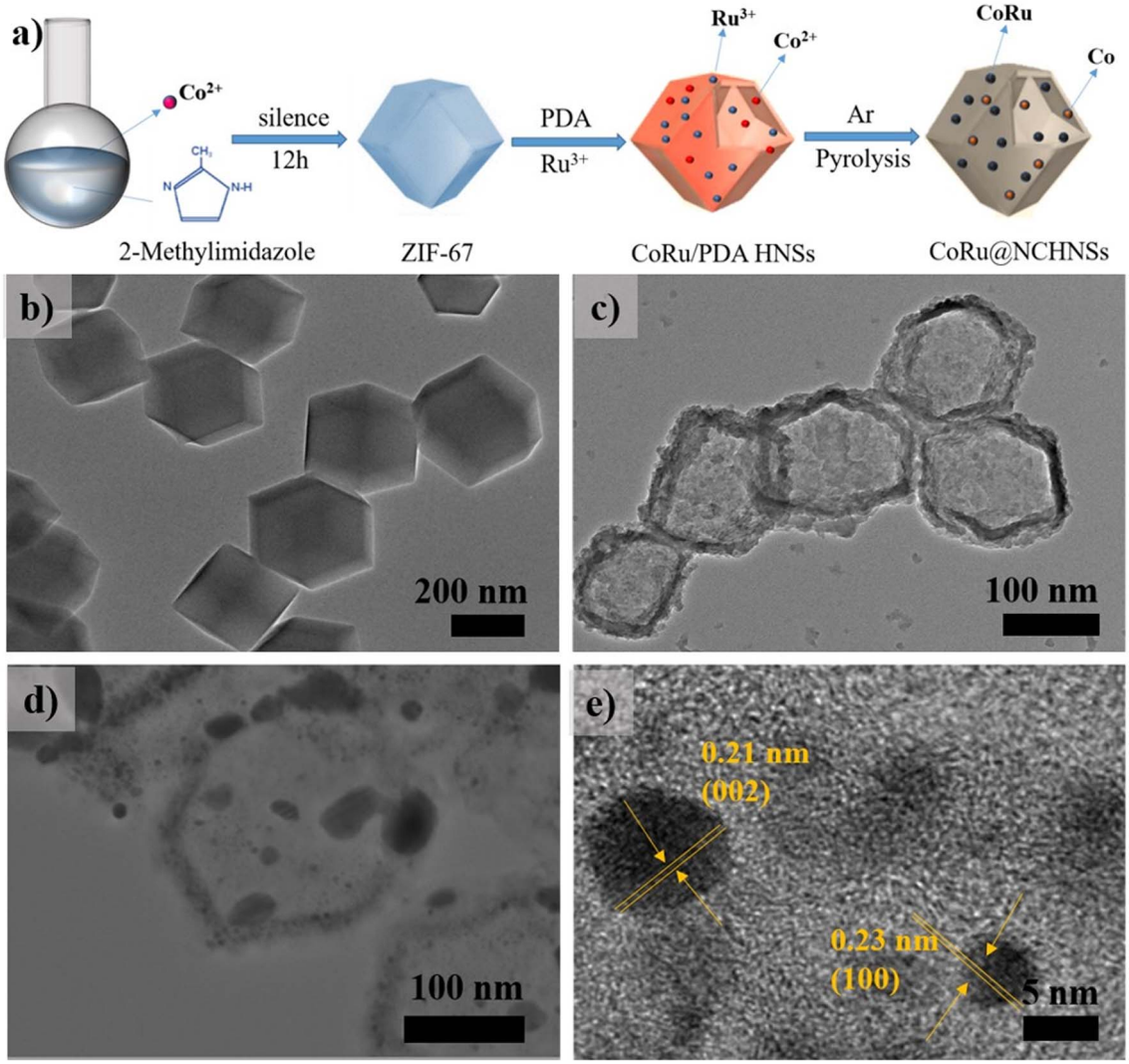

Fig. 1 (a) Schematic illustration of the synthesis of the CoRu@NCHNSs, (b–d) TEM images of ZIF-67, CoRu/PDA HNSs-9 h and CoRu@NCHNSs-9 h, and (e) HR-TEM image of CoRu@NCHNSs-9 h.

binding energy than ZnRu@NCHNSs-9 h (Fig. S8a†).[52,53] This indicated that the electronic interaction between Co and Ru was stronger than that between Zn and Ru.

Furthermore, XRD was subsequently performed to investigate the composition and crystalline structure of the catalysts (Fig. 3). It could be found that CoRu/PDA HNSs-9 h did not maintain the crystalline structure of the original ZIF-67, and a diffuse scattering peak could be clearly observed at ~20°, which was attributed to the amorphous polymer PDA.[23] After pyrolysis at 750 °C, the signal peak of Co@NCHNSs-9 h at 44.2° corresponds well to the cubic Co (PDF# 15-0806) (111) facet, while CoRu/PDA HNSs-9 h exhibited another peak at 45.8° corresponding to the (101) facet of hexagonal CoRu (PDF# 65-8976), indicating that CoRu/PDA HNSs-9 h had not only cubic Co but also hexagonal CoRu, and the introduction of ruthenium could change cubic Co crystallinity to hexagonal CoRu. There were no obvious signal peaks of crystalline Ru which indicated that Ru mostly formed a CoRu alloy. The XRD signal peaks of ZnRu@NCHNSs-9 h correspond well to hexagonal Ru (PDF# 89-4903), which indicated that Ru^{3+} was mostly transformed into Ru nanoparticles in the ZnRu@NCHNSs-9 h catalyst (Fig. S9†).

Hydrogen evolution reaction

The HER catalytic activity of different catalysts was measured in 1 M KOH solution at room temperature using a typical three-electrode system without iR-correction. The linear sweep voltammetry (LSV) curves of all samples are illustrated in Fig. 4a. CoRu@NCHNSs-9 h showed the best HER catalytic activity in a basic electrolyte; it could reach a current density of 10 mA cm^{-2} (η10) at an overpotential of 13 mV, which was lower than that of ZnRu@NCHNSs-9 h of 18 mV and much lower than that of Co@NCHNSs-9 h of 118 mV. This indicated that the introduction of Ru can greatly improve the HER catalytic activity, the Ru site was the intrinsic active site of the HER and the synergistic effect of the CoRu alloy was better than that of the ZnRu alloy. The performance comparison of the materials at different

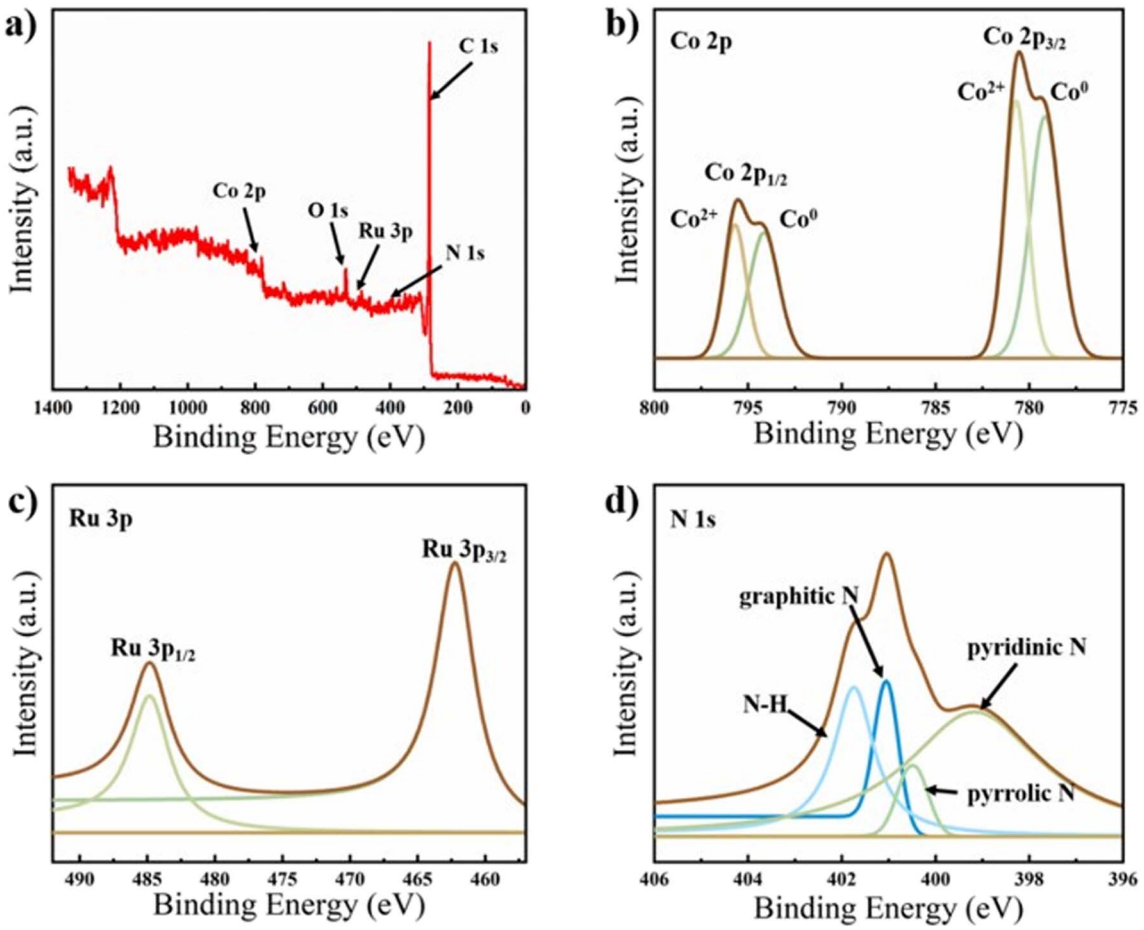

Fig. 2 (a) Survey scan of CoRu@NCHNSs-9 h and (b–d) high-resolution XPS spectra of Co 2p, Ru 3p, and N 1s.

reaction times showed that CoRu@NCHNSs-8 h, CoRu@NCHNSs-9 h and CoRu@NCHNSs-10 h showed a volcano-type trend, with a large degree of decay at 10 h, mainly due to the destruction of the hollow structure. This further showed that the hollow structure played an important role in the catalytic performance of materials. It was noteworthy that the HER activity of CoRu@NCHNSs-9 h in alkaline media was particularly excellent among those of already reported highly efficient HER electrocatalysts (Table S1†).

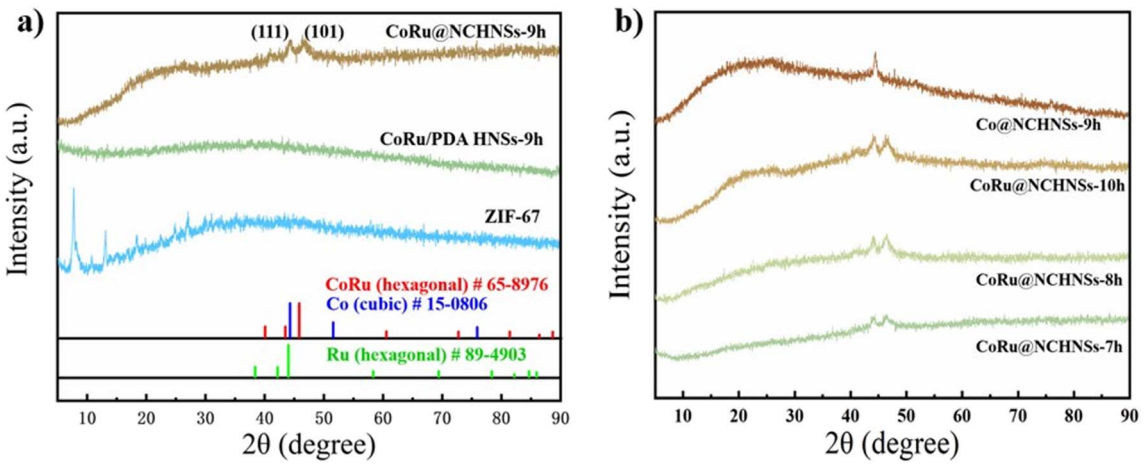

Fig. 3 (a) XRD patterns of ZIF-67, CoRu/PDA HNSs-9 h and CoRu@NCHNSs-9 h and (b) XRD patterns of CoRu@NCHNSs-7 h, CoRu@NCHNSs-8 h, CoRu@NCHNSs-10 h and Co@NCHNSs-9 h.

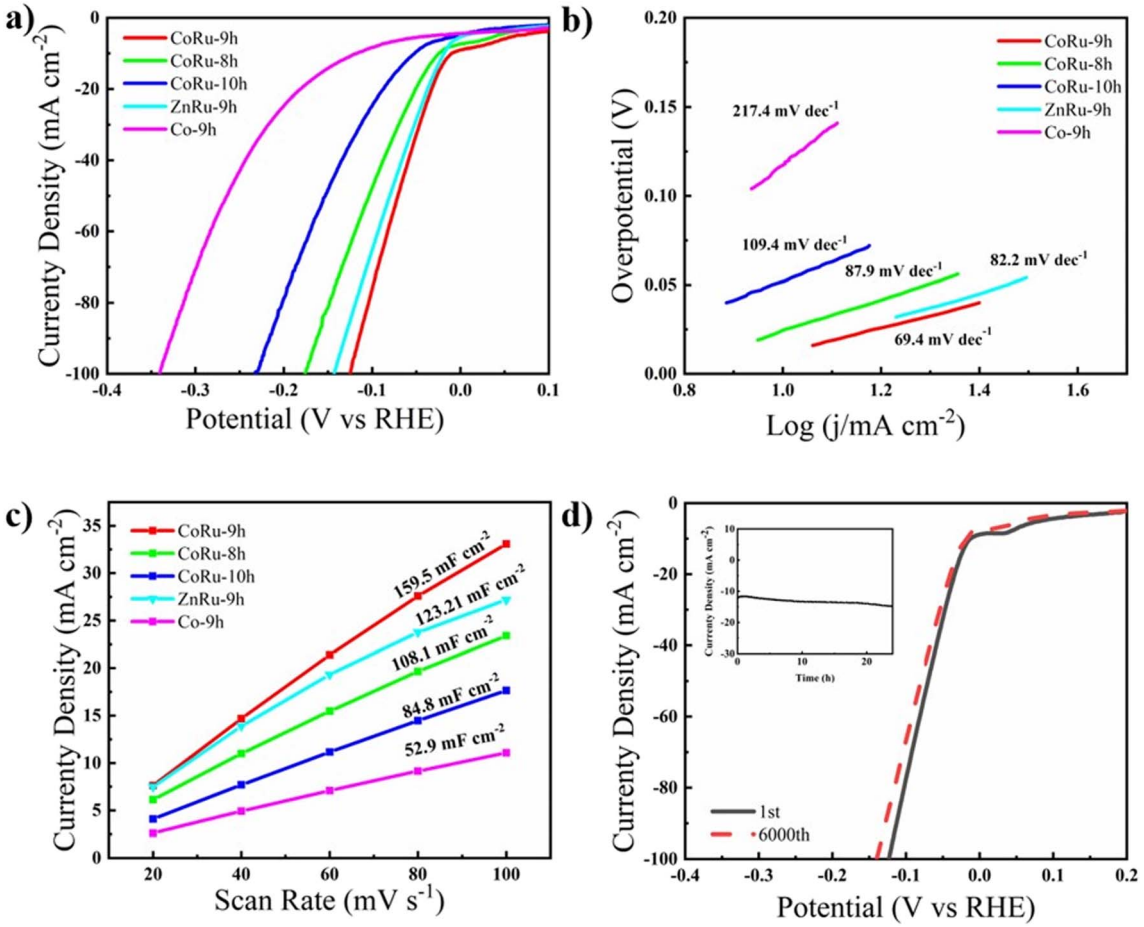

Fig. 4 (a) LSV curves of different samples for the HER in 1 M KOH, (b) corresponding Tafel curves, (c) capacitive currents against the scan rate and corresponding C_{dl} value, and (d) HER stability test of CoRu@NCHNSs-9 h.

In addition, the CoRu@NCHNSs-9 h catalyst exhibited the smallest Tafel slope of only 69.4 mV dec^{-1}, which indicated optimal HER kinetics (Fig. 4b).[54] The electrode kinetics of the catalyst during the HER was investigated by electrochemical impedance spectroscopy (EIS),[55,56] and the semicircle in the mid-frequency range reflected the charge transfer resistance (R_{ct}) (Fig. S10†). The smallest R_{ct} of CoRu@NCHNSs-9 h showed ideal electron transfer and catalytic kinetics, which corresponds to the smallest Tafel slope. The electrochemically active surface area (ECSA) was evaluated by using the double layer capacitance (C_{dl}),[57] which could be obtained by cyclic voltammetry (CV) at different scan rates from 20–100 mV s^{-1} (Fig. S11†). CoRu@NCHNSs-9 h had the largest C_{dl} value of 159.5 mF cm^{-2} (Fig. 4c). More importantly, the specific activity curves normalized by ECSA[58] further confirmed that CoRu@NCHNSs-9 h has the best intrinsic activity (Fig. S12a†). Furthermore, the turnover frequency (TOF) was calculated to evaluate the intrinsic HER activity[59] (Fig. S12b†). CoRu@NCHNSs-9 h has a maximum TOF value of 0.0054 s^{-1} at a potential of −0.1 V (Fig. S12c†). The polarization curves before and after 6000 cycles were obtained by accelerated continuous cyclic voltammetry (CV) scans, which only displayed a slight decay. In addition, in a long-cycle chronoamperometry test, the current density could almost be maintained in the initial state after 24 h, indicating that the CoRu@NCHNSs-9 h catalyst had excellent stability (Fig. 4d). The original morphology and crystalline structure were maintained according to the TEM image and XRD pattern of CoRu/PDA HNSs-9 h after the HER (Fig. S13 and S14†).

Oxygen evolution reaction

Using a similar process to the HER, the OER performance of the materials was tested. The CoRu@NCHNSs were found to have the same competitiveness as OER catalysts. As shown in Fig. 5a, it was obvious that CoRu@NCHNSs-8 h showed the best performance with a current density of 10 mA cm^{-2} at an overpotential of 238 mV (Table S2†), while CoRu@NCHNSs-7 h and CoRu@NCHNSs-9 h showed 280 mV and 289 mV, respectively (Table S2†). However, ZnRu@NCHNSs-9 h had almost no catalytic performance, and the result of Co@NCHNSs-9 h was also not good ($\eta 10 = 450$ mV). It was revealed that the Co site was the intrinsically active site of the OER and the synergistic effect of the CoRu alloy greatly improved the OER catalytic performance. Correspondingly, the CoRu@NCHNSs-8 h catalyst also exhibited the smallest Tafel slope value of 240.71 mV dec^{-1} (Fig. 5b) and the smallest charge transfer resistance (R_{ct}, Fig. S15†). Cyclic voltammetry (CV) at different scan rates was also used to

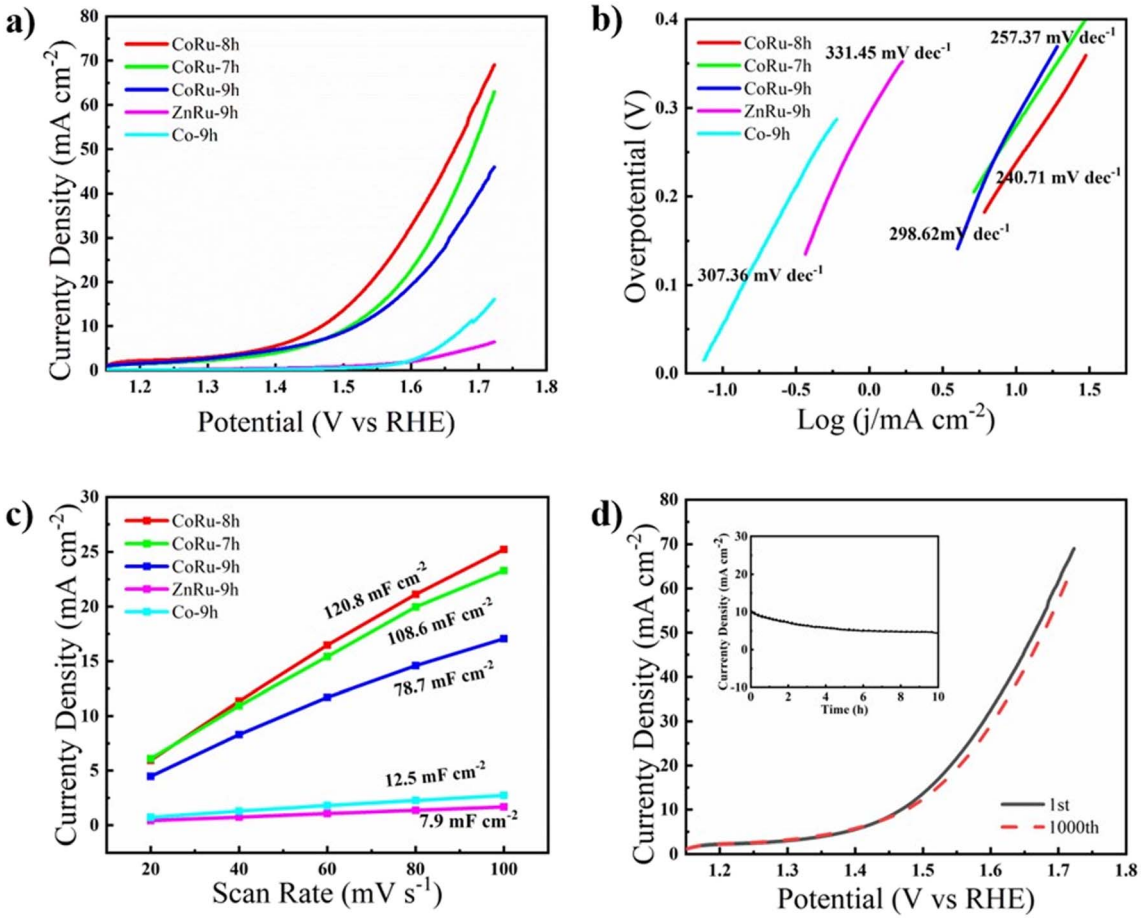

Fig. 5 (a) LSV curves of different samples for the OER in 1 M KOH, (b) corresponding Tafel curves, (c) capacitive current against the scan rate and corresponding C_{dl} value, and (d) OER stability test of CoRu@NCHNSs-8 h.

evaluate the electrochemically active surface area (ECSA) of the material (Fig. S16†), and CoRu@NCHNSs-8 h still had the maximum C_{dl} value of 85 mF cm^{-2} (Fig. 5c). The specific activity curves and TOF curves normalized by ECSA are shown in Fig. S17.† The material stability was tested by cyclic voltammetry (CV) and chronoamperometry. Only a slight decay occurred after 1000 cycles and 10 h, implying good stability (Fig. 5d).

To find the reason why CoRu@NCHNSs-9 h had the best HER performance and CoRu@NCHNSs-8 h had the best OER

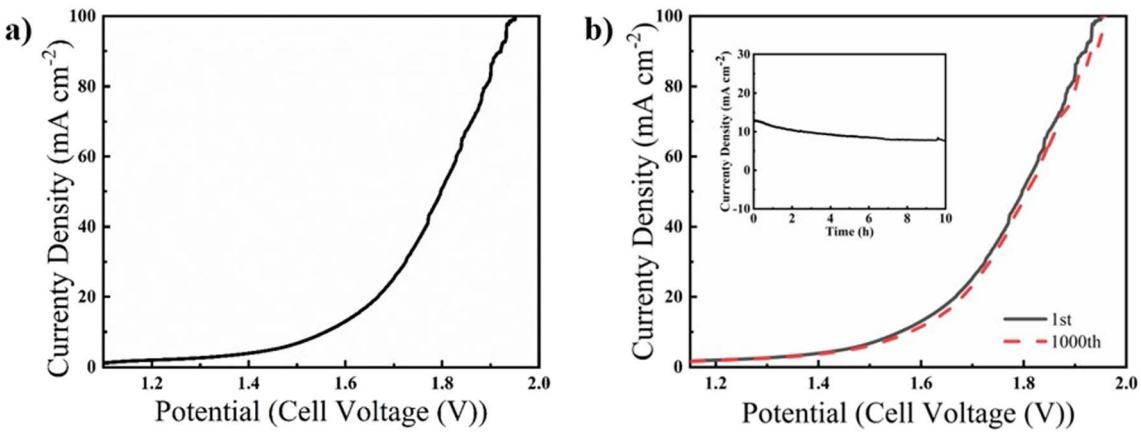

Fig. 6 (a) LSV curve of CoRu@NCHNSs-8 h and CoRu@NCHNSs-9 h as the anode and cathode in 1.0 M KOH for overall water splitting in a two-electrode system and (b) stability test for overall water splitting.

performance, both materials were tested using ICP-OES, and it can be seen that the content of Ru in CoRu@NCHNSs-9 h was much more than that in CoRu@NCHNSs-8 h, while the content of Co in CoRu@NCHNSs-8 h was higher than that in CoRu@NCHNSs-9 h (Table S3†). This indicated that Ru had a greater effect on the HER, while Co had a greater effect on the OER, which further proved our previous assumptions. The original morphology and crystalline structure were still maintained according to the TEM image and XRD pattern of CoRu@NCHNSs-8 h after the OER (Fig. S18 and S19†).

Overall water splitting

Based on the excellent catalytic activity of CoRu@NCHNSs for both the OER and HER in 1 M KOH aqueous solution, the overall water splitting performance was tested using CoRu@NCHNSs-8 h and CoRu@NCHNSs-9 h as the anode and cathode of a two-electrode system. A cell voltage of only 1.56 V was required to achieve a current density of 10 mA cm^{-2}. Excellent overall hydrolytic activity was exhibited (Fig. 6a and Table S4†). The LSV curve showed only a slight decay after 1000 cycles; the performance showed almost no obvious changes after 10 h of chronoamperometric testing in 1 M KOH, indicating excellent stability (Fig. 6b).

Conclusions

In this paper, a novel hollow structure material loaded with the CoRu alloy is prepared by a ligand competition-induced polymerization. Thanks to the synergistic effect of the CoRu alloy, the unique hollow structure and the introduction of N atoms, the CoRu@NCHNSs exhibit excellent HER, OER and overall water splitting performance with a current density of 10 mA cm^{-2} at overpotentials of 13 mV, 240 mV and 1.56 V, respectively. This work explores the application of the CoRu alloy in overall water splitting, and CoRu@NCHNSs possess remarkable HER performance and good OER and overall water splitting performance, which provides a new idea for the preparation of efficient electrocatalytic overall water splitting materials.

Conflicts of interest

The authors declare that they have no conflict of interest.

Acknowledgements

This work was supported by the National Natural Science Foundation of China (Grant no 21774045).

References

1 H. Dotan, A. Landman, S. W. Sheehan, K. D. Malviya, G. E. Shter, D. A. Grave, Z. Arzi, N. Yehudai, M. Halabi, N. Gal, N. Hadari, C. Cohen, A. Rothschild and G. S. Grader, *Nat. Energy*, 2019, **4**, 786–795.
2 G. Zhang, Y.-S. Feng, W.-T. Lu, D. He, C.-Y. Wang, Y.-K. Li, X.-Y. Wang and F.-F. Cao, *ACS Catal.*, 2018, **8**, 5431–5441.
3 Y. Shi and B. Zhang, *Chem. Soc. Rev.*, 2016, **45**, 1529–1541.
4 R. Wu, B. Xiao, Q. Gao, Y. R. Zheng, X. S. Zheng, J. F. Zhu, M. R. Gao and S. H. Yu, *Angew. Chem., Int. Ed.*, 2018, **57**, 15445–15449.
5 J. Zhang, T. Wang, D. Pohl, B. Rellinghaus, R. Dong, S. Liu, X. Zhuang and X. Feng, *Angew. Chem., Int. Ed.*, 2016, **55**, 6702–6707.
6 F. Song, L. Bai, A. Moysiadou, S. Lee, C. Hu, L. Liardet and X. Hu, *J. Am. Chem. Soc.*, 2018, **140**, 7748–7759.
7 J. S. Kim, B. Kim, H. Kim and K. Kang, *Adv. Energy Mater.*, 2018, **8**, 1702774.
8 X. Zhao, P. Pachfule, S. Li, J. R. J. Simke, J. Schmidt and A. Thomas, *Angew. Chem., Int. Ed.*, 2018, **57**, 8921–8926.
9 J. Feng, F. Lv, W. Zhang, P. Li, K. Wang, C. Yang, B. Wang, Y. Yang, J. Zhou, F. Lin, G. C. Wang and S. Guo, *Adv. Mater.*, 2017, **29**, 1703798.
10 V. Petrykin, K. Macounova, O. A. Shlyakhtin and P. Krtil, *Angew. Chem., Int. Ed.*, 2010, **49**, 4813–4815.
11 J. Lin, P. Wang, H. Wang, C. Li, X. Si, J. Qi, J. Cao, Z. Zhong, W. Fei and J. Feng, *Adv. Sci.*, 2019, **6**, 1900246.
12 X. Shi, X. Ling, L. Li, C. Zhong, Y. Deng, X. Han and W. Hu, *J. Mater. Chem. A*, 2019, **7**, 23787–23793.
13 C.-N. Lv, L. Zhang, X.-H. Huang, Y.-X. Zhu, X. Zhang, J.-S. Hu and S.-Y. Lu, *Nano Energy*, 2019, **65**, 103995.
14 L. Yang and L. Zhang, *Appl. Catal. B-Environ.*, 2019, **259**, 118053.
15 P. Xiao, W. Chen and X. Wang, *Adv. Energy Mater.*, 2015, **5**, 1500985.
16 T. Zhou, J. Bai, Y. Gao, L. Zhao, X. Jing and Y. Gong, *J. Colloid Interface Sci.*, 2022, **615**, 256–264.
17 G. Ou, P. Fan, H. Zhang, K. Huang, C. Yang, W. Yu, H. Wei, M. Zhong, H. Wu and Y. Li, *Nano Energy*, 2017, **35**, 207–214.
18 Z. Zheng, L. Lin, S. Mo, D. Ou, J. Tao, R. Qin, X. Fang and N. Zheng, *Small*, 2018, **14**, 1800759.
19 L. Yin, X. Du, C. Di, M. Wang, K. Su and Z. Li, *Chem. Eng. J.*, 2021, **414**, 128809.
20 Y. Wang, S. Wang, Z. L. Ma, L. T. Yan, X. B. Zhao, Y. Y. Xue, J. M. Huo, X. Yuan, S. N. Li and Q. G. Zhai, *Adv. Mater.*, 2022, **34**, 2107488.
21 M. Zhang, J. Wang, L. Ma and Y. Gong, *J. Colloid Interface Sci.*, 2022, **628**, 299–307.
22 S. Yang, F. Jiao and Y. Gong, *Sep. Purif. Technol.*, 2024, **331**, 125716.
23 Y. Chen, M. Wang, S. Xiang, J. Liu, S. Feng, C. Wang, N. Zhang, T. Feng, M. Yang, K. Zhang and B. Yang, *ACS Sustain. Chem. Eng.*, 2019, **7**, 10912–10919.
24 H. Zhang, J. Diao, M. Ouyang, H. Yadegari, M. Mao, M. Wang, G. Henkelman, F. Xie and D. J. Riley, *ACS Catal.*, 2023, **13**, 1349–1358.
25 Z. W. Seh, J. Kibsgaard, C. F. Dickens, I. Chorkendorff, J. K. Nørskov and T. F. Jaramillo, *Science*, 2017, **355**, aad4998.
26 X. Xiao, X. Wang, X. Jiang, S. Song, D. Huang, L. Yu, Y. Zhang, S. Chen, M. Wang, Y. Shen and Z. Ren, *Small Methods*, 2020, **4**, 1900796.
27 D. Chen, R. Lu, Z. Pu, J. Zhu, H.-W. Li, F. Liu, S. Hu, X. Luo, J. Wu, Y. Zhao and S. Mu, *Appl. Catal. B-Environ.*, 2020, **279**, 119396.

28 T. Feng, G. Yu, S. Tao, S. Zhu, R. Ku, R. Zhang, Q. Zeng, M. Yang, Y. Chen, W. Chen, W. Chen and B. Yang, *J. Mater. Chem. A*, 2020, **8**, 9638–9645.
29 K. Shah, R. Dai, M. Mateen, Z. Hassan, Z. Zhuang, C. Liu, M. Israr, W. C. Cheong, B. Hu, R. Tu, C. Zhang, X. Chen, Q. Peng, C. Chen and Y. Li, *Angew. Chem., Int. Ed.*, 2021, **61**, 2114951.
30 Z. Liu, X. Yang, G. Hu and L. Feng, *ACS Sustain. Chem. Eng.*, 2020, **8**, 9136–9144.
31 X. Li, D. Luo, F. Jiang, K. Zhang, S. Wang, S. Li, Q. Zha, Y. Huang and Y. Ni, *Small*, 2023, **19**, 2301850.
32 Y. Zhang, R. Lu, C. Wang, Y. Zhao and L. Qi, *Adv. Funct. Mater.*, 2023, **33**, 2303073.
33 T. Lee, Y. Park, H. Kim, Y. K. Hong, E. Hwang, M. Kim, S. K. Kim and D. H. Ha, *Int. J. Energy Res.*, 2022, **46**, 7975–7987.
34 X. Cao, L. Gao, J. Qu, L. Li, Y. Xie, Y. Zhao, G. Wang and H. Liu, *Small*, 2023, **19**, 2302639.
35 R. Qin, P. Wang, Z. Li, J. Zhu, F. Cao, H. Xu, Q. Ma, J. Zhang, J. Yu and S. Mu, *Small*, 2021, **18**, 2105305.
36 Y. Wang, W. Luo, H. Li and C. Cheng, *Nanoscale Adv.*, 2021, **3**, 5068–5074.
37 Y. Lai, W. Xia, J. Li, J. Pan, C. Jiang, Z. Cai, C. Wu, X. Huang, T. Wang and J. He, *Electrochim. Acta*, 2021, **375**, 137966.
38 Z. Huang, Z. Yang, Q. Jia, N. Wang, Y. Zhu and Y. Xia, *Nanoscale*, 2022, **14**, 4726–4739.
39 X. Sun, J. Jiang, Y. Yang, Y. Shan, L. Gong and M. Wang, *ACS Appl. Mater. Interfaces*, 2019, **11**, 19132–19140.
40 C. Zhao, Y. Zhang, L. Chen, C. Yan, P. Zhang, J. M. Ang and X. Lu, *ACS Appl. Mater. Interfaces*, 2018, **10**, 23731–23739.
41 S. Xiang, H.-J. Qian, Y. Chen, K. Zhang, Y. Shi, W. Liu, H. Sun, H. Sun and B. Yang, *Chem. Mater.*, 2017, **29**, 6536–6543.
42 S. Xiang, D. Wang, K. Zhang, W. Liu, C. Wu, Q. Meng, H. Sun and B. Yang, *Chem. Commun.*, 2016, **52**, 10155–10158.
43 Y. Yang, Z. Lun, G. Xia, F. Zheng, M. He and Q. Chen, *Energy Environ. Sci.*, 2015, **8**, 3563–3571.
44 L. Du, L. Luo, Z. Feng, M. Engelhard, X. Xie, B. Han, J. Sun, J. Zhang, G. Yin, C. Wang, Y. Wang and Y. Shao, *Nano Energy*, 2017, **39**, 245–252.
45 A. Sivanantham, P. Ganesan, L. Estevez, B. P. McGrail, R. K. Motkuri and S. Shanmugam, *Adv. Energy Mater.*, 2018, **8**, 1702838.
46 H. Guo, Q. Feng, J. Zhu, J. Xu, Q. Li, S. Liu, K. Xu, C. Zhang and T. Liu, *J. Mater. Chem. A*, 2019, **7**, 3664–3672.
47 Y. Liu, S. Sun, X. Zheng, D. Li, J. Zhu, M. Zhang and D. Jiang, *Inorg. Chem.*, 2022, **61**, 17557–17567.
48 J. Chen, J. Huang, Y. Zhao, L. Cao, K. Kajiyoshi, Y. Liu, Z. Li and Y. Feng, *Chem. Eng. J.*, 2022, **450**, 138026.
49 W. Li, Y. Zhao, Y. Liu, M. Sun, G. I. N. Waterhouse, B. Huang, K. Zhang, T. Zhang and S. Lu, *Angew. Chem., Int. Ed.*, 2020, **60**, 3290–3298.
50 H. Liu, S. Zeng, P. He, F. Dong, M. He, Y. Zhang, S. Wang, C. Li, M. Liu and L. Jia, *Electrochim. Acta*, 2019, **299**, 405–414.
51 M. Qin, S. Fan, X. Li, Z. Yin, L. Wang and A. Chen, *ACS Appl. Mater. Interfaces*, 2021, **13**, 38256–38265.
52 D. Zhao, Z. Li, X. Yu, W. Zhou, Q. Wu, Y. Luo, N. Wang, A. Liu, L. Li and S. Chen, *Chem. Eng. J.*, 2022, **450**, 138254.
53 H. Zhang, H. Su, M. A. Soldatov, Y. Li, X. Zhao, M. Liu, W. Zhou, X. Zhang, X. Sun, Y. Xu, P. Yao, S. Wei and Q. Liu, *Small*, 2021, **17**, 2105231.
54 B. Owens-Baird, Y. V. Kolen'ko and K. Kovnir, *Chem.–Eur. J.*, 2018, **24**, 7298–7311.
55 Y. Li, F.-M. Li, X.-Y. Meng, X.-R. Wu, S.-N. Li and Y. Chen, *Nano Energy*, 2018, **54**, 238–250.
56 H. Sun, Y. Min, W. Yang, Y. Lian, L. Lin, K. Feng, Z. Deng, M. Chen, J. Zhong, L. Xu and Y. Peng, *ACS Catal.*, 2019, **9**, 8882–8892.
57 C. C. L. McCrory, S. Jung, I. M. Ferrer, S. M. Chatman, J. C. Peters and T. F. Jaramillo, *J. Am. Chem. Soc.*, 2015, **137**, 4347–4357.
58 C. Wang and L. Qi, *Angew. Chem., Int. Ed.*, 2020, **59**, 17219–17224.
59 W. Zhou, D. D. Huang, Y. P. Wu, J. Zhao, T. Wu, J. Zhang, D. S. Li, C. Sun, P. Feng and X. Bu, *Angew. Chem., Int. Ed.*, 2019, **131**, 4271–4275.